Supplementary Information (SI) for Journal of Materials Chemistry A.
This journal is © The Royal Society of Chemistry 2024

Supplementary information for

Tailoring of PVDF for retrieval of piezoelectric powders to optimize piezo-catalytic water treatment

Kaiyu Feng[1], Yan Zhang[1*], Xuefan Zhou[1], Yan Zhao[1], Hanyu Gong[1], Xiang Zhou[1], Hang Luo[1], Dou Zhang[1], Chris Bowen[2]

[1] *State Key Laboratory of Powder Metallurgy, Central South University, Changsha, 410083, China*

[2] *Department of Mechanical Engineering, University of Bath, United Kingdom, Bath BA2 7AY, UK*

S1. Fabrication of BNT ($Bi_{0.5}Na_{0.5}TiO_3$) nanofibers:

BNT nanofibers were synthesized using an electrospinning technology. Sodium acetate ($C_2H_3NaO_2$, ≥99%, Sino-pharm Chemical Reagent Co., Ltd) and bismuth acetate ($C_6H_9BiO_6$, ≥99%, Sino-pharm Chemical Reagent Co., Ltd) were dissolved in a mixed solvent of 2-methoxyethanol ($C_3H_8O_2$, AR, Sino-pharm Chemical Reagent Co., Ltd) and glacial acetic acid ($C_2H_4O_2$, AR, Sino-pharm Chemical Reagent Co., Ltd) with a volume ratio of 1:1 in a 1:1 molar ratio to form a uniform solution; this will be referred to as Solution A. Solution B was prepared by dissolving titanium butoxide ($C_{16}H_{36}O_4Ti$, CR, Sino-pharm Chemical Reagent Co., Ltd) in acetylacetone ($C_5H_8O_2$, AR, Sino-pharm Chemical Reagent Co., Ltd) with a molar ratio of 1:2. Subsequently, Solution B was slowly poured into Solution A, and the mixture was stirred at 60°C for 12 hours to obtain the precursor solution of BNT with a concentration of 0.4 M. Before the electrospinning process, 5% by mass of polyvinyl pyrrolidone (PVP, K88-96, Shanghai Macklin Biochemical Co., Ltd) was added to the precursor solution. The composite solution was loaded into a plastic syringe.

The electrospinning process was performed using an electrospinning system (JDF05, Changsha Nano-apparatus Ltd.co, China) using a voltage of 12 kV and a feed rate of 1 mL/h. The environmental temperature during electrospinning was approximately 35 ~ 45 °C, with a relative humidity not exceeding 20%. The collector drum had a diameter of 8 cm and rotated at 800 rpm. To facilitate the collection of nanofibers on the drum, the distance between the needle and the collector drum was approximately 10 cm. The collected nanofibers were dried at 70 °C for 24 hours, heated at 325 °C for 1 hour, and then calcined with a heating rate of 3 °C/min to a temperature of 700 °C.

S2. Fabrication of BFO ($BiFeO_3$) polyhedrons:

Equal molar ratios of $Fe(NO_3)_3 \cdot 9H_2O$ (Shanghai Macklin Biochemical Co., Ltd) and $Bi(NO_3)_3 \cdot 5H_2O$ (Shanghai Macklin Biochemical Co., Ltd) were added to 30 ml of deionized water. After stirring for half an hour, a 7M KOH (Shanghai Aladdin Biochemical Technology Co., Ltd) solution was gradually added, leading to a final mixed solution of 60 ml. The mixed solution was poured into a reaction vessel with a polytetrafluoroethylene lining and reacted at 200 °C for 4 hours. The obtained powders were washed several times with deionized water and dried in an oven at 60 °C for 12 hours.

S3. Fabrication of BST ($Ba_{0.75}Sr_{0.25}TiO_3$) nanospheres:

BST nanospheres were synthesized using a hydrothermal method. 5 g polyethylene glycol 6000 (PEG 6000, AR, Shanghai Macklin Biochemical Co., Ltd) were added to 14 ml anhydrous ethanol. After completely dissolving PEG 6000 through a process of ultrasonic dispersion, Solution C was obtained. A mass of 0.32 g of barium hydroxide octahydrate ($Ba(OH)_2 \cdot 8H_2O$, AR, Shanghai Macklin Biochemical Co., Ltd) and a mass of 0.07 g of strontium hydroxide octahydrate ($Sr(OH)_2 \cdot 8H_2O$, ≥99%, Shanghai Titan Scientific Co., Ltd) were combined and added to a small glass bottle containing 7.1 ml of deionized water. The mixture was stirred on a magnetic stirring plate for half an hour, to form a uniform solution referred to as Solution D 0.4 ml butyl titanate ($Ti(OC_4H_9)_4$, , ≥99%, Shanghai Macklin Biochemical Co., Ltd) was dissolved in 9.6 ml anhydrous ethanol to form Solution E. To Solution C, 10 ml of 5 mol/L Potassium hydroxide (KOH, ≥90%, Shanghai Titan Scientific Co., Ltd) ethanol solution was added. During the stirring process, Solutions D and E were added dropwise into the beaker one after the other. After thorough mixing, the combined solution was transferred to a 100 ml stainless steel reaction vessel that was lined with polytetrafluoroethylene. The reaction was carried out at 180 °C for 24 hours. After filtration, the lower layer powders were obtained. The powder was washed twice with deionized water, acetic acid, and anhydrous ethanol. After drying in a 70 °C oven for 12 hours, the BST nanospheres was obtained.

S4. Fabrication of BIT ($Bi_4Ti_3O_{12}$) nanosheets

The BIT nanosheets were prepared by a molten salt method. A mass of 5.648g of Bi_2O_3 (Shanghai Macklin Biochemical Co., Ltd), 1.467g of TiO_2 (Shanghai Macklin Biochemical Co., Ltd), 14.054g of NaCl (Shanghai Aladdin Biochemical Technology Co., Ltd), and 17.928g of KCl (Shanghai Aladdin Biochemical Technology Co., Ltd) were placed in a ball milling jar with zirconia balls, and anhydrous ethanol was used as the milling medium. The mixture was ball-milled in a planetary ball mill at a speed of 250 rpm for 24 hours. The resulting powders were then calcined at 740 °C for 2 hours at a heating rate of 5°C per minute. After cooling to room temperature, the powders were washed repeatedly with hot water to remove residual salts and subsequently cleaned three times with deionized water and ethanol.

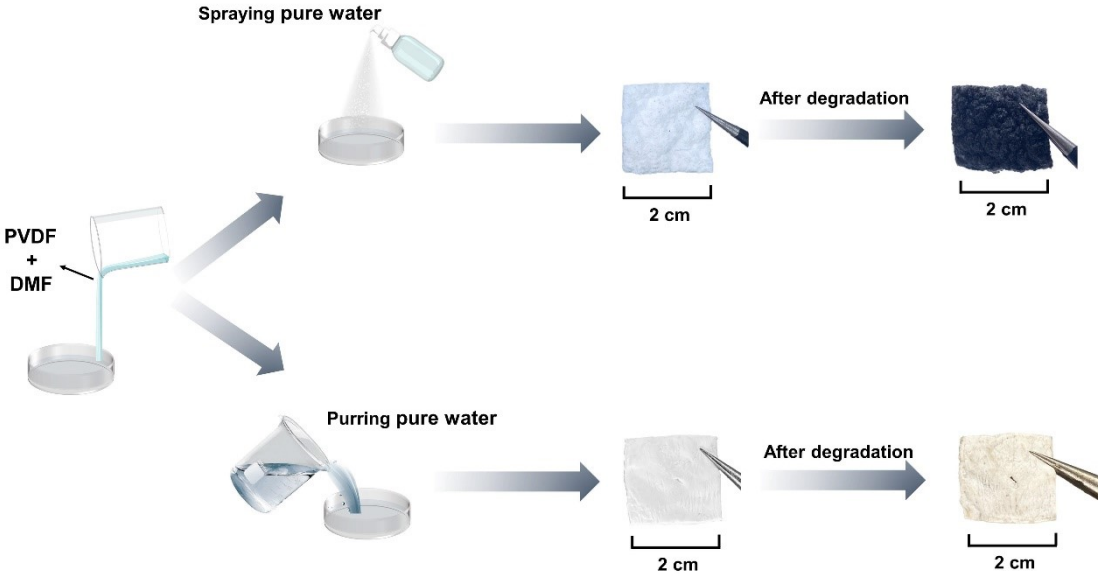

Fig. S1. BT@PDA powders anchored on the rough and smooth surface of PVDF.

Polyvinylidene fluoride (PVDF) was dissolved in N, N-Dimethylformamide (DMF), and the viscous solution was poured into a culture dish. Subsequently, PVDF with rough surface was obtained by a solvent exchange process through spraying deionized water onto the culture dish. However, if water is directly poured slowly into the culture dish, the surface of PVDF is smooth. It can be found that rough-surfaced PVDF captures more BT@ polydopamine (BT@PDA) and become darker in color, while a smooth-surfaced PVDF can only capture a small amount of BT@PDA (almost still white in color).

In a common solvent exchange process, when PVDF was fully dissolved in DMF, pure water was poured in for solvent exchange, and a shaped PVDF is obtained after drying. This type of PVDF exhibited a porous structure, but the surface is smooth, which is not conducive to capturing the BT@PDA powders. With the same ultrasound conditions, this type of PVDF binds a small amount of BT@PDA (Fig. S1). However, the PVDF prepared by solvent evaporation method exhibited a dense and smooth surface. With the same ultrasound conditions, almost no BT@PDA powders can be found on the PVDF (Fig. S2). This indicates that the rough PVDF surface can be loaded with a greater mass of powders compared to the smooth PVDF, since the rough surface provides more binding sites[1]. In addition, the porous PVDF can load more BT@PDA powders compared to the dense PVDF, as the ultrasound facilitates the formation of negative pressure within the pore space[2], thereby allowing the BT@PDA powders to contact with PVDF easily and form hydrogen bonding.

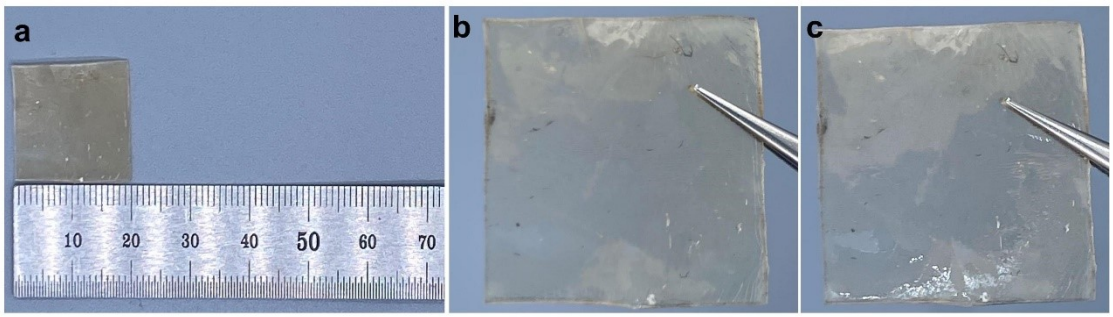

Fig. S2. (a) PVDF prepared by solvent evaporation method. Comparison of PVDF before (b) and after (c) recovery experiment.

PVDF prepared by solvent evaporation method: A mass of 2g PVDF particles was added into a 20ml DMF solution and stirred at 60°C for 4 hours to obtain a mixture of PVDF and DMF. Then, the mixture was poured into a petri dish and allowed to sit in air for 24 hours in order to allow the solvent to evaporate to produce a film.

PVDF prepared by the solvent evaporation method has a harder texture, exhibits a transparent nature, and has a smooth and dense surface; these characteristics render the PVDF prepared by this method incapable of efficiently retrieving powders.

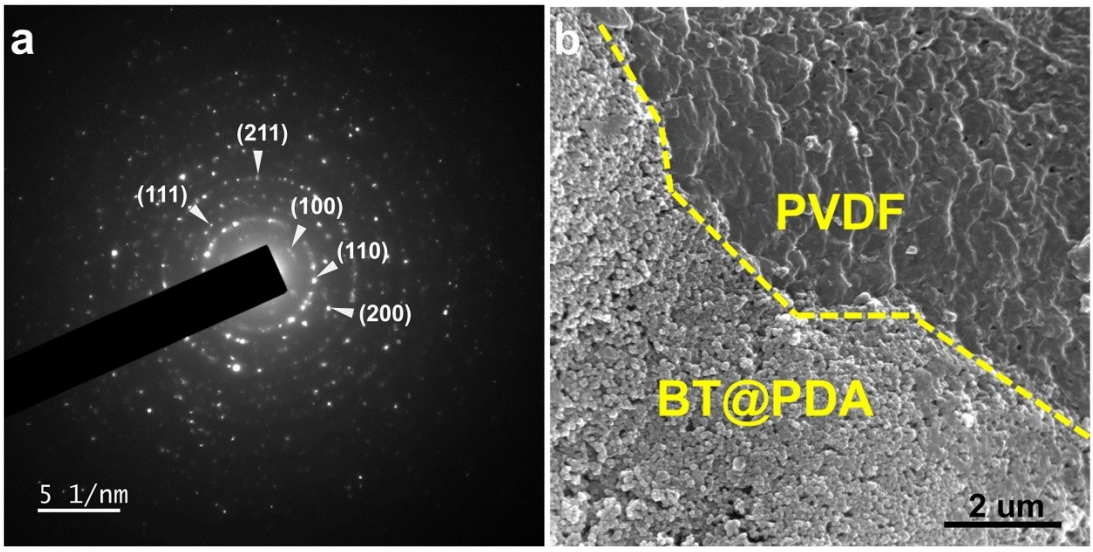

Fig. S3. (a) Selected area electron diffraction (SAED) pattern of BT@PDA. (b) Scanning electron microscopy (SEM) images of BT@PDA/PVDF.

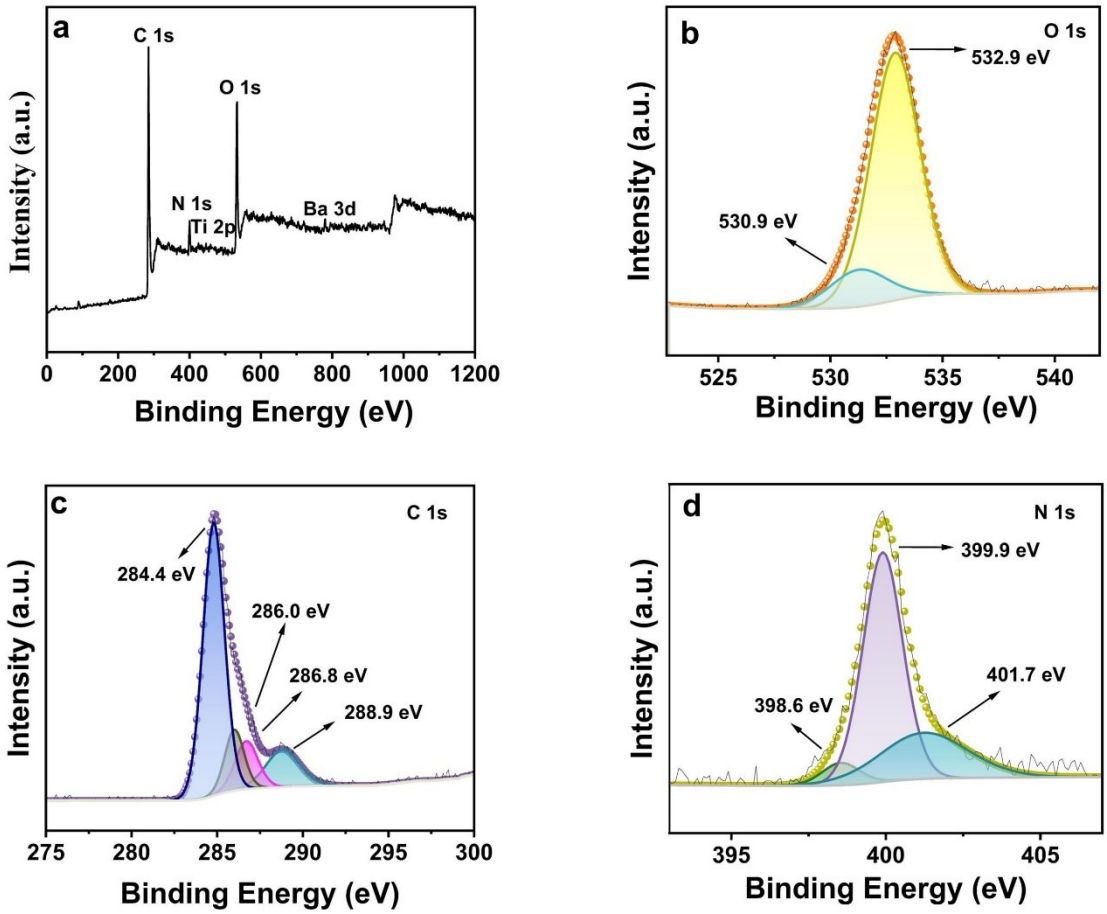

Fig. S4. (a) XPS wide-scan spectra of BT@PDA. XPS high-resolution spectra for (b) O 1s, (c) C 1s and (d) N 1s of BT@PDA.

In the C 1s spectrum (Fig. S4c), four peaks were fitted at 284.4, 286.0, 286.8, and 288.9 eV, corresponding to C-C, C-N, C-O, and O-C=O bonds, respectively[3]. Combined with Raman spectroscopy, it can be inferred that the generation of carbon defects may be related to the interaction between dopamine and the interface of barium titanate. In the N 1s spectrum (Fig. S4d), three peaks were fitted at 398.6, 399.9, and 401.7 eV, corresponding to -N=, -NH-, and $-NH_2$ bonds[4], respectively, providing evidence for the presence of dopamine in BT@PDA.

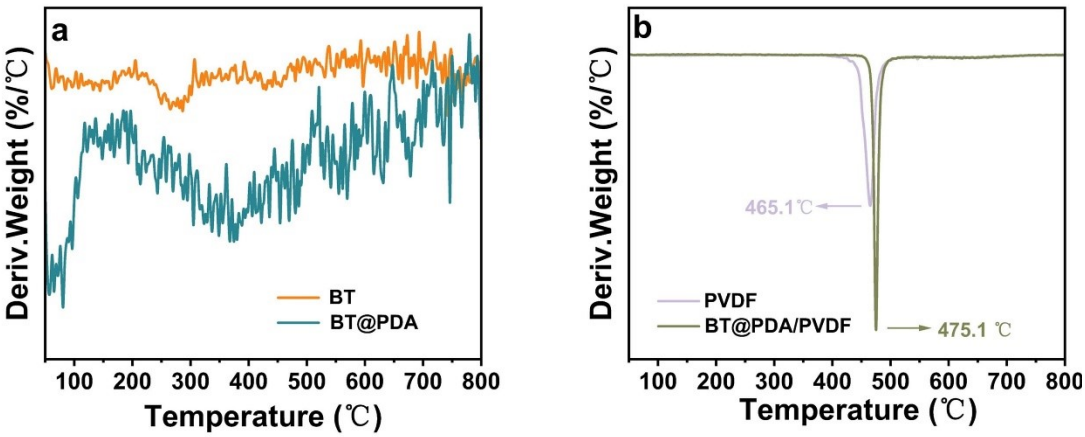

Fig. S5. Derivative thermogravimetry (DTG) of (a) BT and BT@PDA, (b) PVDF and BT@PDA/PVDF.

As shown in Fig. S5a, the rate of thermal decomposition of BT@PDA is higher than that of BT within the measured temperature range. This is attributed to the decomposition of polydopamine at high temperatures. Furthermore, compared to BT@PDA/PVDF, pure PVDF begins its thermal decomposition at a lower temperature. This is because the initial stage of decomposition primarily involves PVDF, and the BT@PDA loaded on PVDF absorbs a small amount of heat, thereby delaying the degradation of BT@PDA/PVDF. As the temperature reaches approximately 470 °C, BT@PDA a rapid decomposition of BT@PDA/PVDF was observed (Fig. S5b).

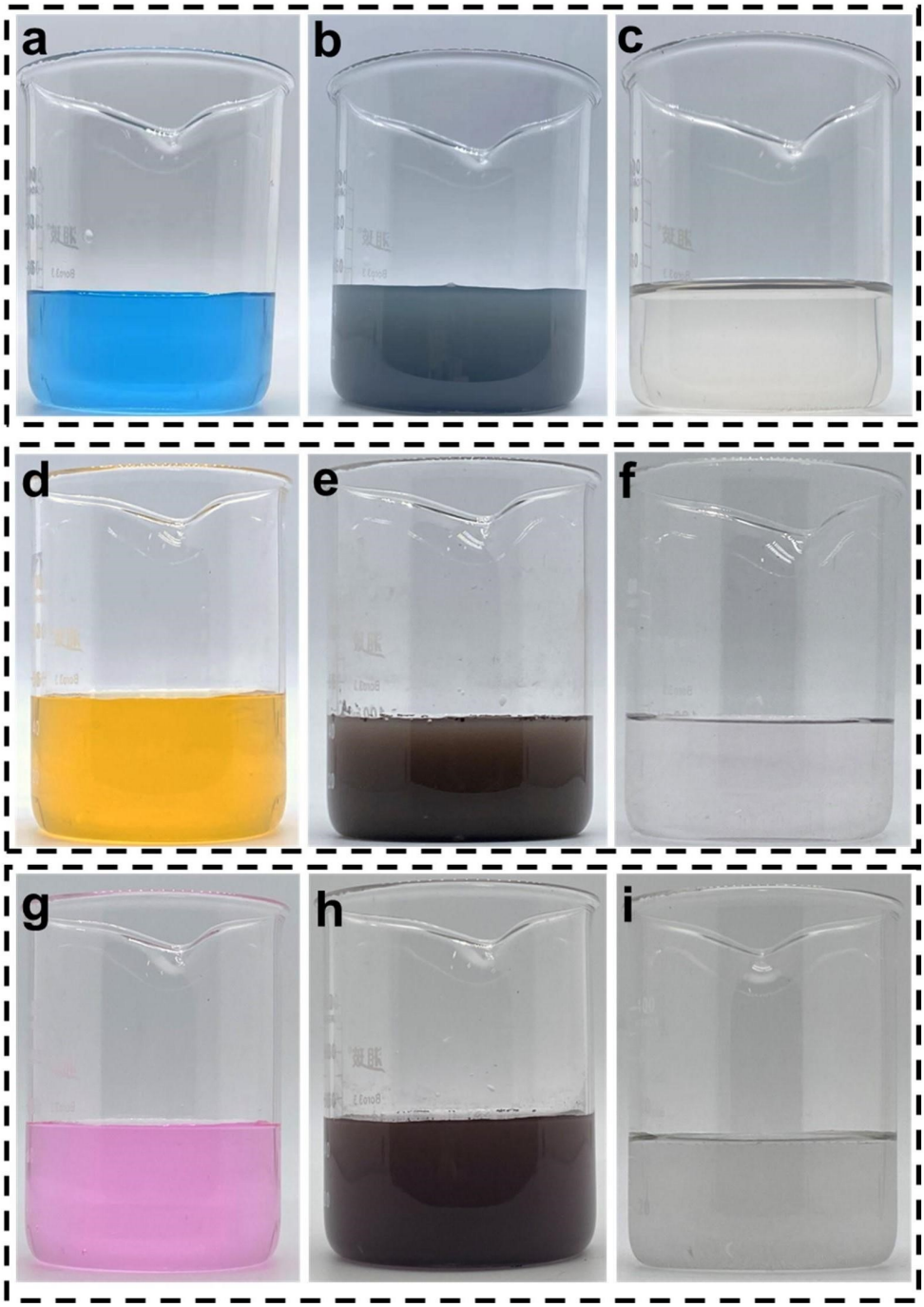

Fig. S6. BT@PDA powders and PVDF for different dye degradation.

Fig. S6a, d and g show optical images of the pristine Indigo Carmine (IC), Methyl Orange (MO) and Rhodamine B (RhB) solution. After adding BT@PDA and PVDF, the color of solutions deepened, as shown in Fig. S6b, e and h. The clean solutions shown in Fig. S6c, f and i were obtained after piezocatalysis with ultrasound applied for 70 min, followed by removal of the bulk BT@PDA/PVDF.

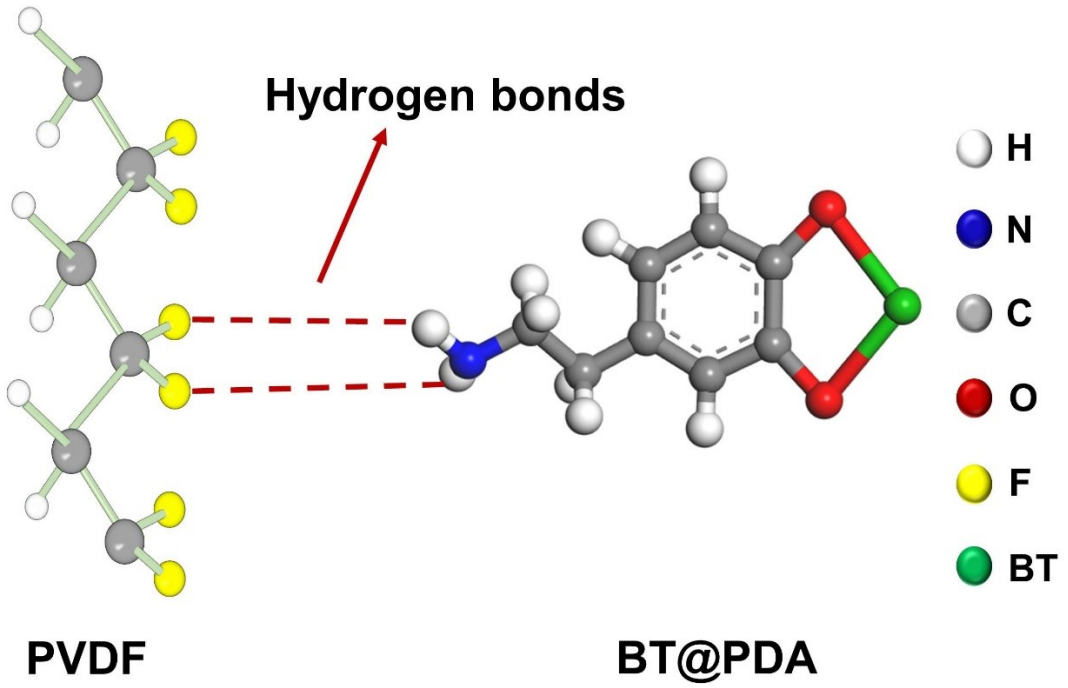

Fig. S7. Interfacial interactions between BT@PDA and PVDF via hydrogen bonds.

Periodic molecular dynamics (MD) simulations of the material system were carried out[5]. First, 40 PVDF chains and 28 BT@PDA were simulated, in which each PVDF chain was composed of 5 monomers. Ba may be connected to one or two hydroxyl groups in dopamine. Here, we assumed that the two cases were equal. COMPASS force fields were applied to PVDF and BT@PDA via the FORCITE module and a check was made to ensure that the overall charge is 0[6]. All simulations were conducted with a time step of 1fs. After that, PVDF and BT@PDA AC boxes were built, whereby geometric optimization of AC boxes was carried out to ensure that the overall energy was at a minimum level. The result of geometric optimization is convergent, indicating that no further annealing operation is required. The FORCITE module was used for molecular dynamics simulation with the time step set at 1fs and the temperature set at 300 K. Geometric optimization and molecular dynamics are carried out under COMPASS force field. The RDF data is computed by the FORCITE module based on the previous settings.

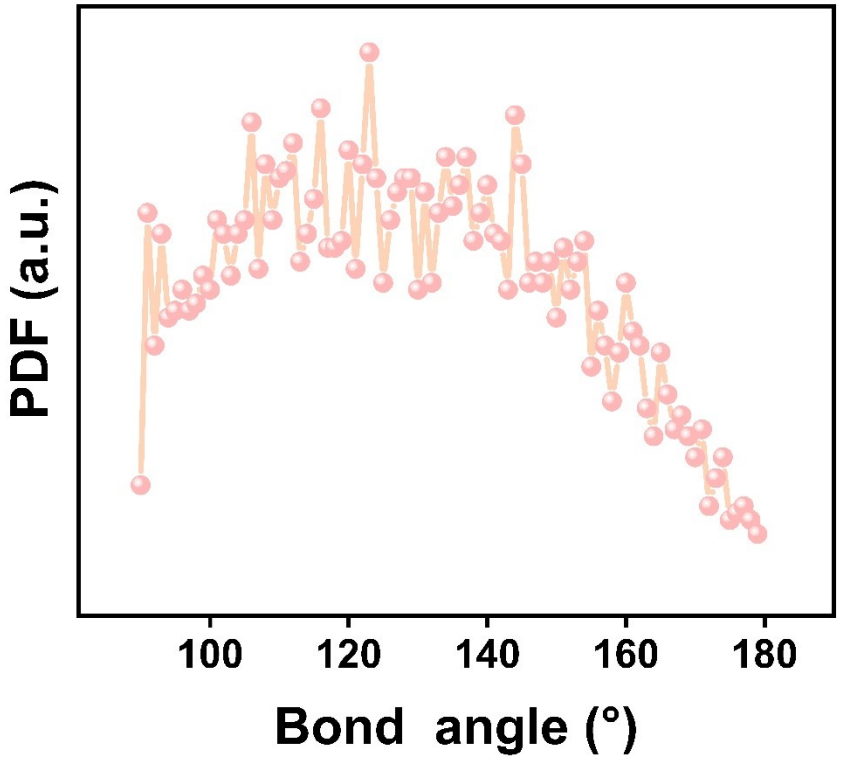

Fig. S8. Probability density function (PDF) of bond angles of hydrogen bonds in AC boxes.

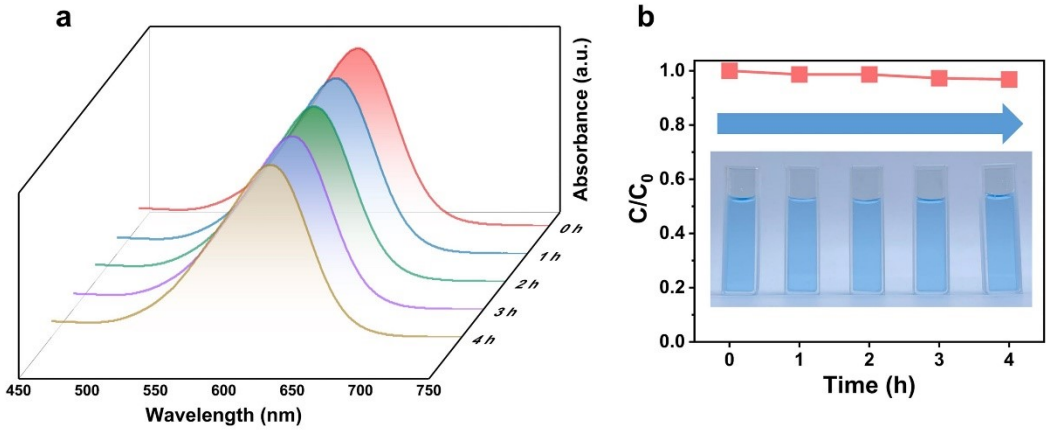

Fig. S9. (a) UV-vis spectra of the IC solution using BT@PDA as the catalyst with a condition of stirring. (b) C_0/C-time curve of dye degradation with the inset as the optical image of IC dye; where C_0 is initial concentration of the dye, C is the concentration of the dye after degradation.

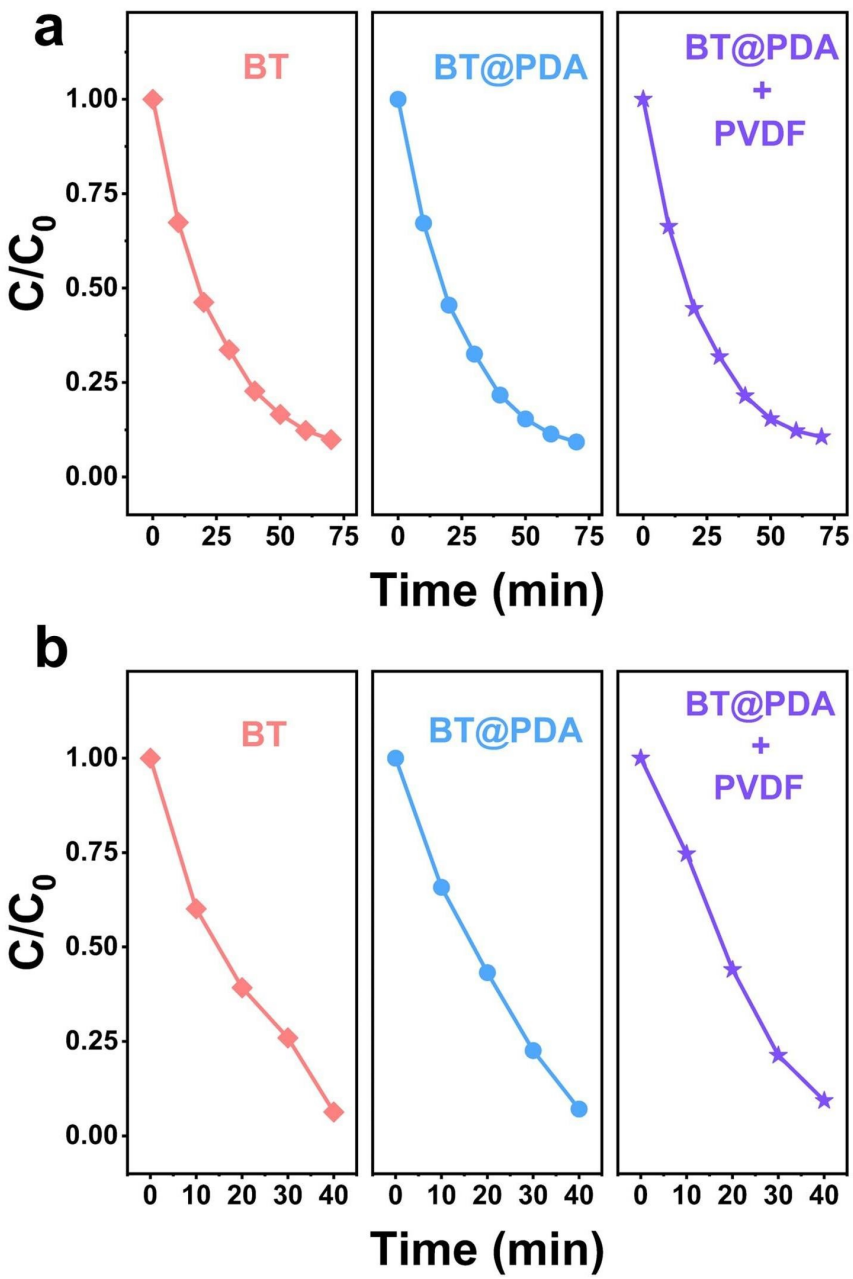

Fig. S10. Piezocatalytic degradation curves of (a) RhB and (b) MO;

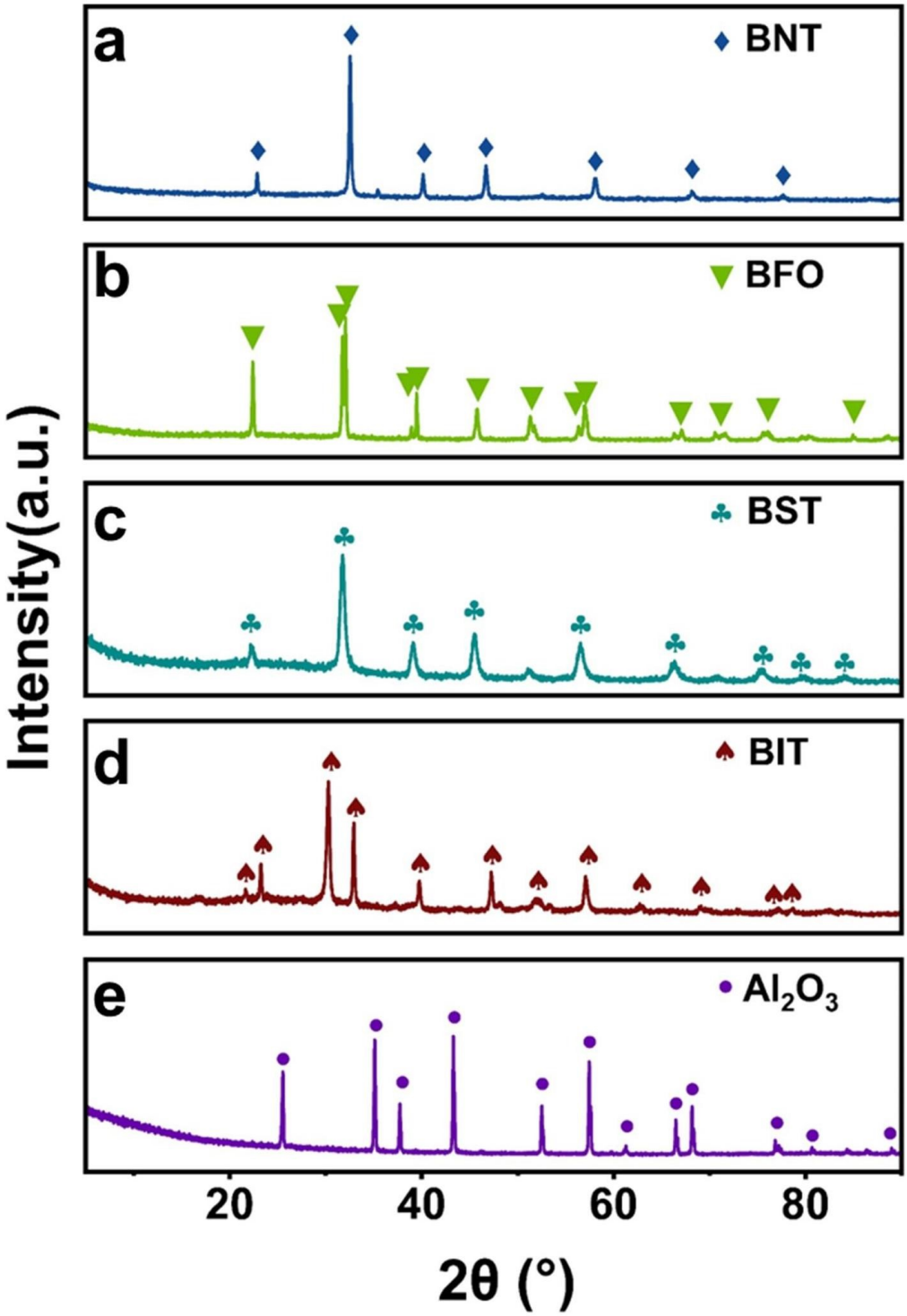

Fig. S11. X-ray diffraction (XRD) patterns of (a) BNT, (b) BFO, (c) BST, (d) BIT and (e) Al_2O_3;

Fig. S11 shows the X-ray diffraction patterns of five different powders. The fabrication methods of BNT, BFO, BST and BIT were illustrated in S1-4. An Al_2O_3 powder was purchased from Shanghai

Aladdin Biochemical Technology Co., Ltd. Correct phase structures without impurity were observed.

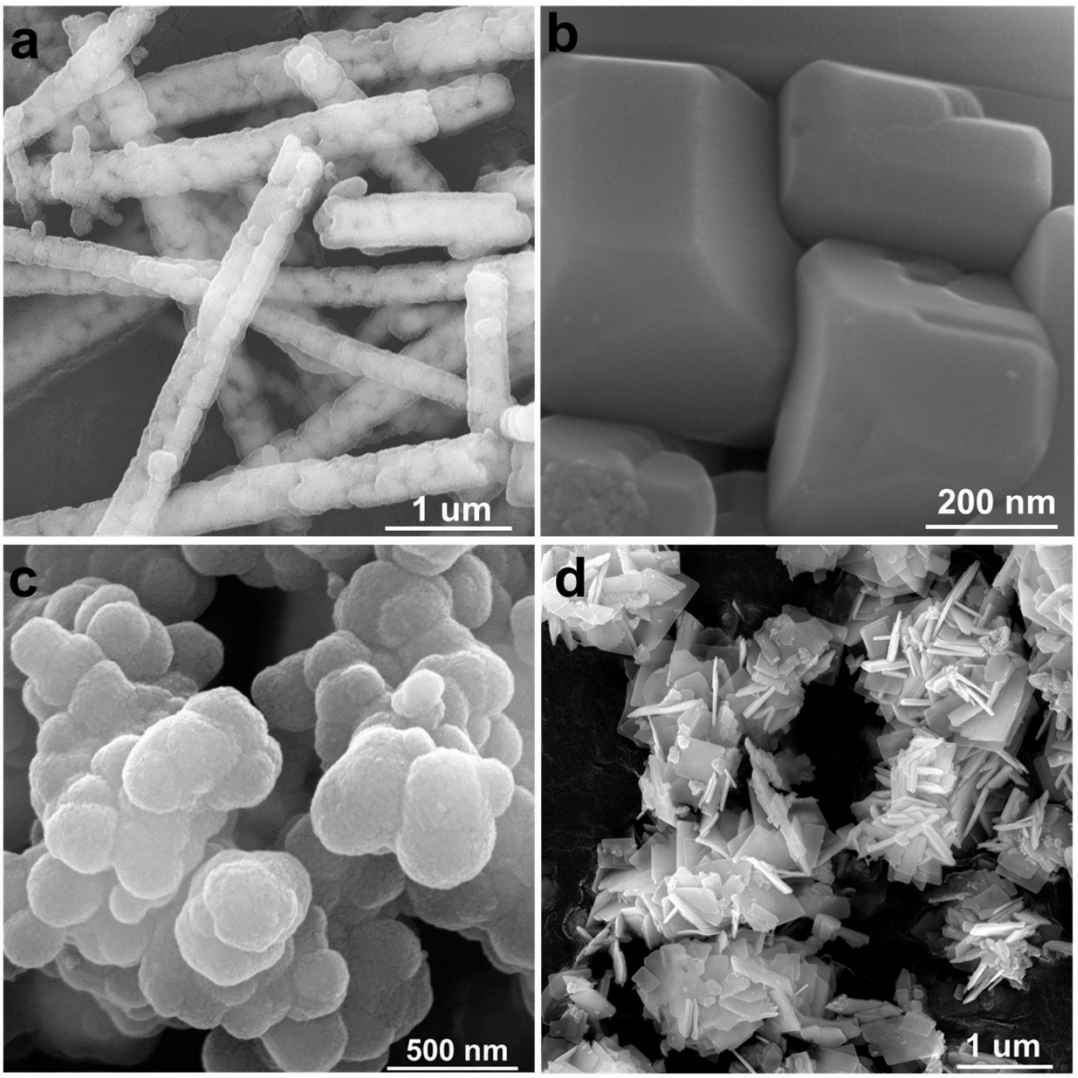

Fig. S12. SEM images of (a) BNT, (b) BFO, (c) BST, (d) BIT.

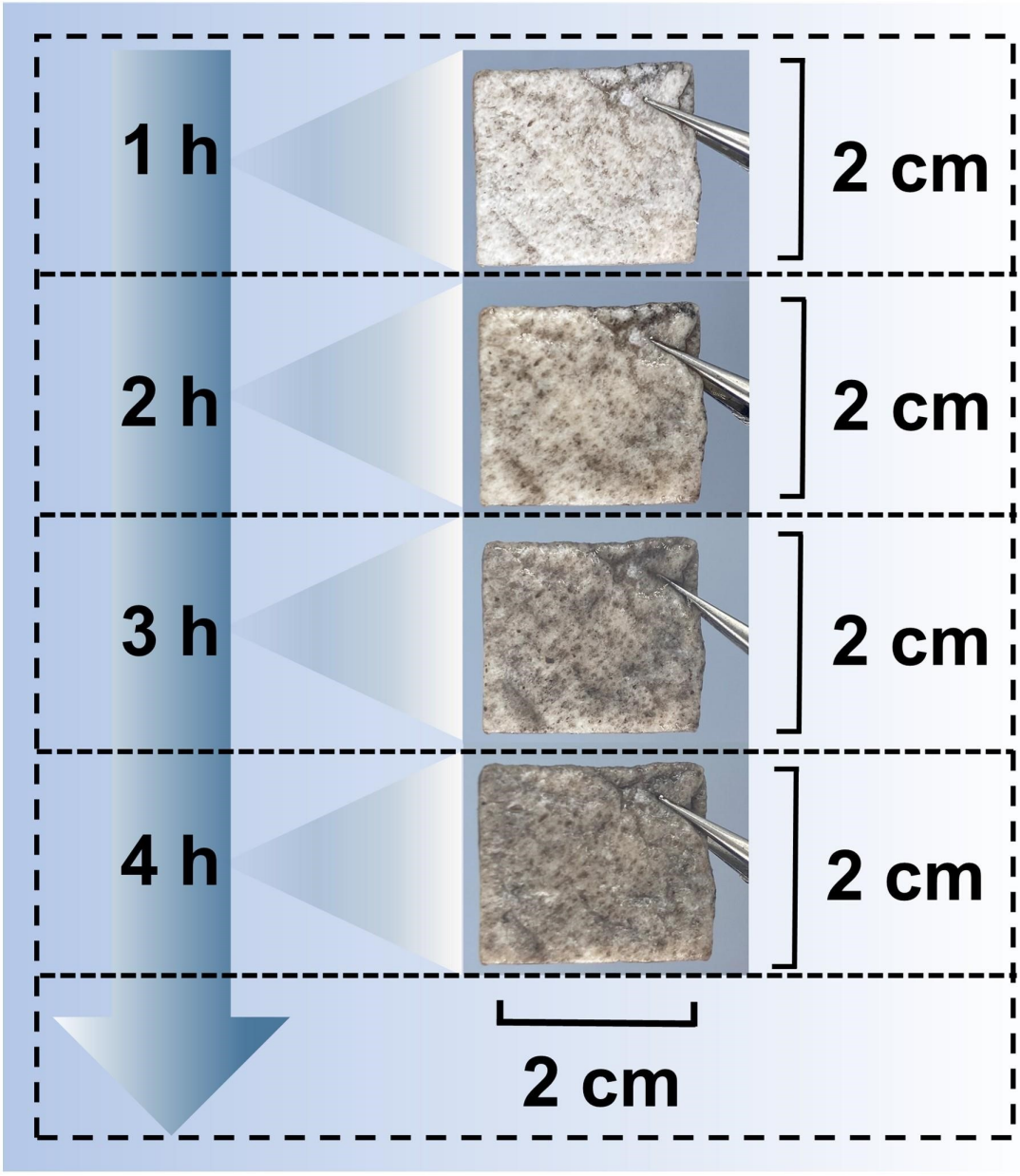

Fig. S13. Loading condition of PVDF with BT@PDA under stirring conditions.

Fig. S13 shows the optical images of BT@PDA/PVDF extracted from the solution with a condition of stirring. When the stirring time was extended from 1 to 4 hours, the color of the BT@PDA/PVDF gradually deepened.

Table S1. Integral areas of pair correlation functions curves between the $-CF_2$ groups (in PVDF) and the $-NH_2$ and -OH groups (in dopamine).

Integral area	**2.0-3.0 (Å)**	**3.0-5.0 (Å)**
O-H---F	0.35	1.69
N-H---F	0.19	1.73

Table S2. Recent typical catalytic performances of piezocatalysts include both retrievable and irretrievable catalysts.

Piezocatalyst	Condition	Pollutants	Property	Retrievability	Ref.
BIT-Nd	Ultrasonic	RhB	97.3% within 15 min	Unachievable	[7]
BIT-OV1	Ultrasonic	RhB	100% within 60 min	Unachievable	[8]
Bi_2WO_6	Ultrasonic	RhB	99% within 100 min	Unachievable	[9]
$BaTiO_3$	Ultrasonic	IC	81.19% within 45 min	Unachievable	[10]
BTO-PDMS	Ultrasonic	RhB	94% within 120 min	achievable	[11]
BNT/PVDF	Ultrasonic	RhB	76.6% within 180 min	achievable	[12]
KNN6L-PDMS	Ultrasonic	RhB	91% within 180 min	achievable	[13]
BT-TOAR	Ultrasonic	IC	15% within 40 min	achievable	[14]
BT@PDA+PVDF	Ultrasonic	IC	94.3% within 40 min	achievable	This work
BT@PDA+PVDF	Ultrasonic	RhB	90.7% within 40 min	achievable	This work

References

1. F. F. Cao, L. Zhang, H. Wang, Y. W. You, Y. Wang, N. Gao, J. S. Ren and X. G. Qu, *Angew. Chem.-Int. Edit.*, 2019, **58**, 16236-16242.
2. G. Wang, Q. Cui, L. J. Yin, Y. Li, M. Z. Gao, Y. Meng, J. Li, S. D. Zhang and W. Wang, *Sep. Purif. Technol.*, 2020, **244**,115805.
3. D. D. Wang, X. L. Gao, L. M. Zhao, J. Zhou, S. P. Zhuo, Z. F. Yan and W. Xing, *RSC Adv.*, 2018, **8**, 16044-16051.
4. R. Yue, X. Wen, Y. N. Mao, Y. T. Su, Q. Shen, H. Z. Song, H. L. Zhang and X. W. Ba, *J. Mater. Sci.*, 2020, **55**, 17094-17107.
5. S. Plimpton, *J. Comput. Phys.*, 1995, **117**, 1-19.
6. H. Sun, *J. Phys. Chem. B*, 1998, **102**, 7338-7364.
7. Y. Zhao, Y. Zhang, Q. Q. Xu, H. Y. Gong, M. Y. Yan, K. Y. Feng, X. Zhou, X. F. Zhou and D. Zhang, *J. Mater. Chem. A*, 2024, **12**, 1753-1763.
8. Q. Tang, J. Wu, X.-Z. Chen, R. Sanchis-Gual, A. Veciana, C. Franco, D. Kim, I. Surin, J. Pérez-Ramírez, M. Mattera, A. Terzopoulou, N. Qin, M. Vukomanovic, B. J. Nelson, J. Puigmartí-Luis and S. Pané, *Nano Energy*, 2023, **108**, 108202.
9. Z. Kang, E. Lin, N. Qin, J. Wu, B. Yuan and D. Bao, *Environ. Sci.-Nano*, 2021, **8**, 1376-1388.
10. Q. Yi, H. Luo, H. Xiong, Q. Liu, D. Zhai, Q. Sun and D. Zhang, *Ceram. Int.*, 2023, **49**, 39707-39718.
11. W. Qian, K. Zhao, D. Zhang, C. R. Bowen, Y. Wang and Y. Yang, *ACS Appl. Mater. Interfaces*, 2019, **11**, 27862-27869.
12. X. F. Zhou, Q. W. Sun, Z. D. Xiao, H. Luo and D. Zhang, *J. Environ. Chem. Eng.*, 2022, **10**, 108339.
13. X. Cheng, Z. Liu, Q. Jing, P. Mao, K. Guo, J. Lu, B. Xie and H. Fan, *J. Colloid Interface Sci.*, 2023, **629**, 11-21.
14. Q. Liu, Z. Li, J. Li, F. Zhan, D. Zhai, Q. Sun, Z. Xiao, H. Luo and D. Zhang, *Nano Energy*, 2022, **98**, 107267.